Available online at www.sciencedirect.com
ScienceDirect
Journal of Catalysis 252 (2007) 321–334
JOURNAL OF CATALYSIS
www.elsevier.com/locate/jcat

Alumina-, niobia-, and niobia/alumina-supported NiMoS catalysts: Surface properties and activities in the hydrodesulfurization of thiophene and hydrodenitrogenation of 2,6-dimethylaniline

Angela S. Rocha [a], Arnaldo C. Faro Jr. [a], Laetitia Oliviero [b,*], Jacob Van Gestel [b], Françoise Maugé [b]

[a] *Departamento de Físico-Química, Instituto de Química, UFRJ, Ilha do Fundão, CT, Rio de Janeiro, RJ, CEP 21949-900, Brazil*
[b] *Laboratoire Catalyse et Spectrochimie, ENSICAEN, Université de Caen, CNRS, 6, Bd Maréchal Juin, F-14050 Caen, France*

Received 9 July 2007; revised 10 September 2007; accepted 11 September 2007

Available online 31 October 2007

Abstract

The activity of NiMoS catalysts supported on niobia, alumina, and niobia/alumina was compared for the thiophene hydrodesulfurization (HDS) and 2,6-dimethylaniline (2,6-DMA) hydrodenitrogenation (HDN) reactions. To evaluate the acidity of the supports and identify the nature of the sulfide sites, adsorption of 2,6-dimethylpyridine, pyridine, and CO was performed and followed by IR spectroscopy. This study has shown that with niobia as a support, the activity of NiMoS catalysts in thiophene HDS and in HDN of 2,6-DMA was no longer promoted by the synergy between Ni and Mo. The absence of synergy between molybdenum and nickel on niobia can be explained by the strong interaction of each metal with niobia at the expense of interaction with each other. Moreover, it has been shown that on a niobia/alumina support, the formation of the NiMoS phase can be directly linked to the presence of alumina not covered by niobia. However, niobia is an interesting support for the HDN of 2,6-DMA, because it favors the formation of xylene through direct ammonia elimination involving low H_2 consumption. The activity for xylene formation on niobia is linked to the electron-deficient nature of the Mo sulfide site, as demonstrated by CO adsorption followed by IR.

Keywords: Hydrotreatment; NiMo synergy; Niobium; HDS; HDN; IR spectroscopy

1. Introduction

Given the continuing worldwide effort to decrease pollutant emissions, the studies of catalysts for hydrotreatment of fuel fractions from petroleum remain relevant. Catalysts for hydrodenitrogenation (HDN) and hydrodesulfurization (HDS) are fundamental for this purpose, because nitrogen and sulfur compounds in fuels not only cause environmental problems, but also are poisons for other catalysts on which these fractions are treated. For these reasons, the allowable range of nitrogen and sulfur content in fuels will become increasingly restrictive, requiring the development of HDN and HDS catalysts with high activity.

Conventional catalysts for hydrotreatment typically are composed of one group VI transition metal sulfide (MoS_2 or WS_2) promoted by sulfided cobalt or nickel and supported on alumina [1–6]. The acid–base characteristics of the supports play a fundamental role in the activity of these catalysts; several groups have studied modified aluminas as supports in an effort to improve their activity [7].

Fluorine was used to increase the acidity of alumina and amorphous silica alumina; however, the activity of NiMo phase for the HDN reaction was not influenced by this variation in acidity [8]. On the other hand, the addition of boron and phosphorous to $NiMo/Al_2O_3$ catalysts has shown positive effects on hydrocracking and HDS activities [9,10].

Along this line, first niobium was tested as an additive to traditional hydrotreating catalyst systems. Niobium oxide has interesting properties in reactions catalyzed by solid acid [11,12]. The addition of niobia (on surface or in the bulk) to alumina for preparing hydrotreating NiMo/Al catalysts has been reported by Weissman [13]. The enhanced hydrotreating activity with the addition of niobia was attributed to the increase in support

* Corresponding author. Fax: +33 231 452 822.
E-mail address: laetitia.oliviero@ensicaen.fr (L. Oliviero).

0021-9517/$ – see front matter
doi:10.1016/j.jcat.2007.09.012

acidity. Gaborit et al. concluded that niobium as a dopant of an industrial $NiMo/Al_2O_3$ catalyst increased its activity in HDS and hydrogenation (HYD) on high-pressure sulfidation with CS_2 [14]. The authors verified the presence of NbS_2 species, with specific acidic properties. Second, niobia- and alumina-supported Ni, Mo, and NiMo catalysts were tested in HDS and cumene hydrocracking [15]. The higher activity in the HDS reaction of alumina-supported NiMo catalysts compared with that supported on niobia was attributed to the fact that synergy between Ni and Mo sulfides occurred on the alumina-supported catalysts but not on the niobia-supported ones. Finally, Allali et al. [16] prepared niobium sulfide supported on carbon or alumina that had HDS activity and found that the genesis of niobium sulfide phases was strongly dependent on the sulfidation method.

Recently, we studied the activity of molybdenum sulfide catalysts supported on niobia, alumina, and niobia/alumina in the thiophene HDS and 2,6-dimethylaniline (2,6-DMA) HDN reactions. 2,6-DMA Mo catalysts supported on niobia containing supports were more active for the XYL route of 2,6-DMA decomposition that the one supported on alumina. We have shown the correlation between this activity improvement and the modification of the electronic properties of the Mo sulfide phase with the support nature [17]. In the present contribution, we aim to study the effect of the support on the promoting effect of nickel on supported Mo catalysts. Toward this purpose, we prepared NiMo sulfide catalysts supported on niobia, pure alumina, and alumina modified with niobia. Their activity in HDS and HDN reactions were investigated. We also studied the effect of H_2S on the activity of the NiMo sulfide catalysts for 2,6-DMA HDN. To evaluate the acidity of the supports and identify the nature of the sulfide sites, adsorption of 2,6-dimethylpyridine, pyridine, and CO was performed and followed by IR spectroscopy.

2. Experimental

2.1. Preparation of the catalysts

Three supports were used: pure oxides γ-Al_2O_3 and Nb_2O_5 and alumina-supported Nb_2O_5. The alumina was obtained by calcination of a boehmite (PURAL SB RT04/111) at 823 K for 3 h. The niobia was prepared by calcination of niobic acid (provided by CBMM) at 773 K for 4 h. The Nb_2O_5/Al_2O_3 was prepared by incipient wetness impregnation of the alumina with an aqueous solution containing the appropriate amount of a niobium ammonium oxalate complex, $(NH_4)_3[NbO(C_2O_4)_3]$, to obtain a final support with 20 wt% of Nb_2O_5, followed by drying at 393 K for 1 h and calcination at 773 K for 4 h. The 20 wt% of Nb_2O_5 corresponds to around 90% of the monolayer on Al_2O_3 according to an atomic density of 5 Nb nm^{-2} [18].

The NiMo catalysts were prepared using incipient wetness sequential impregnation to obtain catalysts with a total of around 5 metal atoms per nm^2 of support surface area. In this method, first the molybdenum impregnation onto the supports was carried out using an aqueous solution of ammonium heptamolybdate, $(NH_4)_6Mo_7O_{24}{\cdot}4H_2O$, and 6% of hydrogen peroxide, the latter to increase the heptamolybdate solubility. The pH was adjusted to 2 by adding HNO_3, to avoid any precipitation of molybdenum compounds. The resulting solids were dried at 393 K and calcined at 723 K. Then the nickel was incorporated by impregnation with an aqueous solution of nickel nitrate, $Ni(NO_3)_2{\cdot}6H_2O$, dried at 393 K and calcined at 723 K. The nomenclature and nominal composition of the catalysts are presented in Table 1.

Table 1
Composition and textural characteristics of the supports and catalysts

Material	S_{BET}[a] ($m^2\ g_{cat}^{-1}$)	PV[b] ($cm^3\ g_{cat}^{-1}$)	Atomic ratio Ni/(Ni + Mo)	wt% Ni[c]	wt% Mo[c]
Al_2O_3	200	0.57	–	–	–
Mo/Al	175	0.44	0	–	12.9
25% NiMo/Al	171	0.44	0.25	2.0	9.9
50% NiMo/Al	185	0.47	0.50	4.1	6.7
75% NiMo/Al	189	0.48	0.75	6.3	3.5
Ni/Al	179	0.49	1.00	8.7	–
Nb_2O_5/Al_2O_3	179	0.43	–	–	–
Mo/NbAl	130	0.32	0	–	11.7
25% NiMo/NbAl	137	0.33	0.25	1.8	9.0
50% NiMo/NbAl	147	0.35	0.50	3.8	6.1
75% NiMo/NbAl	156	0.37	0.75	5.8	3.1
Ni/NbAl	159	0.38	1.00	7.9	–
Nb_2O_5	26	0.12	–	–	–
Mo/Nb	27	0.13	0	–	2.0
25% NiMo/Nb	26	0.12	0.25	0.3	1.5
50% NiMo/Nb	25	0.10	0.50	0.6	1.0
75% NiMo/Nb	27	0.11	0.75	0.9	0.5
Ni/Nb	31	0.13	1.00	1.2	–

[a] Surface area determined by BET method.
[b] Pore volume.
[c] Introduced by impregnation.

2.2. Catalytic activity measurements

The catalysts were tested by means of two reactions: hydrodesulfurization (HDS) of thiophene and hydrodenitrogenation (HDN) of 2,6-dimethylaniline. The thiophene HDS activity test was carried out in a flow microreactor working at atmospheric pressure and 623 K. Appropriate amounts of catalyst (15–30 mg) were used to keep the conversion <5%. Before the reaction, the catalysts were sulfided *in situ* with 30 mL min^{-1} of H_2S/H_2 (10 vol%) at 623 K (heating rate of 3 K min^{-1}) for 1.5 h. Thiophene was introduced into the reactor by flowing hydrogen (70 mL min^{-1}) through a thiophene saturator maintained at 291 K ($P_{thiophene} = 6920$ Pa) and mixed to 20 mL min^{-1} of H_2S/H_2 (10 vol%). Products were analyzed online using a Varian gas chromatograph equipped with a flame ionization detector (FID) and a CPSIL-5CB capillary column. The specific rate at steady state was calculated as $r_{HDS} = (F/m)X$, where F/m is the molar flow rate of reactant per gram of catalyst and X is the thiophene conversion.

The 2,6-dimethylaniline HDN activity test was carried out in a stainless steel reactor (Sotelem) at 4 MPa and 573 K. Around 0.35–0.40 g of catalyst was first sulfided *in situ* under 60 mL min^{-1} of H_2S/H_2 (10 vol%) at 4 MPa and 623 K (temperature ramp of 3 K min^{-1}) for 2 h. Then the catalyst was cooled under H_2S/H_2 to the reaction temperature, and the H_2S content was adjusted at 1.4% in hydrogen. The liquid feed

(10 vol% 2,6-dimethylaniline, reactant; 80% *n*-heptane, solvent; and 10% *n*-decane, internal standard) was introduced by an HPLC pump and vaporized in the H_2S/H_2 stream. The reaction products were condensed at the reactor exit, and the liquid was analyzed with a Varian gas chromatograph equipped with a CPSIL-5CB capillary column and a FID. No new products besides those observed during 2,6-dimethylaniline decomposition on the alumina-supported catalysts were observed on the niobia-containing catalysts.

The partial pressure of 2,6-dimethylaniline was kept constant at 13 kPa for all experiments. Reaction conditions at steady state were varied by changing the contact time (55–250 h g mol^{-1}) at 56 or 0 kPa of H_2S. We determined the reaction orders in 2,6-dimethylaniline for the hydrogenation (HYD), xylene (XYL), and disproportionation (DIS) routes to be 0, 0, and 0.4, respectively [19]. Activities were expressed by the initial rate.

2.3. Characterization

The supports were analyzed by XRD in a Rigaku Miniflex diffractometer, with Cu$K\alpha$ radiation, at $\lambda = 1.5418$ Å, 30 kV, and 15 mA. Raman characterization of the support was performed under ambient conditions. The spectra were recorded on a Labram 300 Raman spectrometer (Jobin Yvon) equipped with a confocal microscope and a CCD camera. The laser was used at $\lambda = 532$ nm with an energy of 30 mW without filtration. No characterization of the oxide catalysts was performed, because the sulfidation modifies the dispersion of the metal phase [15]. The surface areas and pore volumes of the supports and oxidic precursors were determined using the BET method from nitrogen adsorption data at 77 K in a Micromeritics ASAP 2010 C automated volumetric apparatus. Before the analyses, all samples were treated *in situ* under vacuum at 673 K.

Support acidity was characterized by FTIR spectroscopy of adsorbed CO, pyridine (Py), and 2,6-dimethylpyridine (2,6-DMP). The samples were ground and pressed into self-supported wafers (ca. 10 mg, for a disc of 2 cm^2). The supports were activated *in situ* in the IR cell under vacuum at 723 K for 4 h. After activation, 133 Pa of Py or 2,6-DMP was introduced into the cell at ambient temperature. After adsorption, the sample was evacuated at increasing temperatures up to 673 K. Details of the experiments were given previously [20]. Carbon monoxide IR experiments were recorded after the same surface pretreatment and subsequent cooling at 100 K. Small calibrated doses of CO were introduced into the IR cell up to an equilibrium pressure of 133.3 Pa. The system was subsequently evacuated at 100 K down to a residual pressure of 10^{-3} Pa.

Sulfided catalysts were characterized by FTIR of adsorbed CO. The oxidic catalysts were pressed into self-supported wafers (ca. 10 mg, for discs of 2 cm^2) and placed into a quartz IR cell equipped with CaF_2 windows and a cryogenic chamber. Before the adsorption experiments, the samples were sulfided *in situ*, according to the following procedure. The catalysts were evacuated from room temperature up to 623 K, then contacted at 623 K for 1 h with 13.3 kPa of a gas mixture containing 10 vol% H_2S in H_2. After a rapid evacuation of the gas phase, a second dose of H_2S/H_2 mixture was placed in contact with the catalyst overnight. Finally, a third dose of H_2S/H_2 mixture was contacted with the catalyst for 1 h, after which the catalyst was evacuated at the same temperature for 45 min and cooled to 100 K. The subsequent procedure for CO adsorption was the same as for the supports.

Spectra were recorded in 256 scans using a Nicolet FTIR spectrometer. The bands of adsorbed species were obtained by subtracting to the spectra recorded after that recorded before introduction of the probe. Band intensities were corrected for slight differences in the weight of the wafer and normalized to a disc of 5 mg cm^{-2}.

3. Results

3.1. Textural and structural characteristics

The preparation of niobia on alumina is not an easy task, because the common niobium compounds are poorly soluble, and sequential impregnations are required to obtain supports well covered with niobium oxide. This procedure often generates poorly dispersed niobia.

The surface areas and pore volumes of the supports and catalysts for the present study are presented in Table 1. The high surface area of the alumina contrasts with the low surface area of niobia. The niobia/alumina showed only a small decrease in surface area compared with the pure alumina.

The NiMo catalysts on γ-Al_2O_3 and Nb_2O_5/Al_2O_3 exhibited smaller surface areas than their respective supports; this decrease can be explained mainly by the increased catalyst density due to incorporation of the metals. Support pore blockage by metal particles also can contribute to this decreas in surface area. It appears that the pore blockage occurred preferentially with Mo. With Ni, incorporation into the alumina structure would explain a smaller effect [15]. The interpretation is somehow more difficult for the Nb_2O_5 support, because for Mo or Ni catalysts, the pore volume is larger than that of the pure niobia. Impregnation of the metal phase in acidic media could be a reason for redissolution and reprecipitation of the support.

XRD indicated the presence of hexagonal Nb_2O_5 phase (TT-Nb_2O_5) in niobia and of γ-alumina for Nb_2O_5/Al_2O_3 and Al_2O_3 supports, as reported previously [17]. These results corroborate the BET results and strongly indicate preservation of the alumina structure after niobium deposition.

The Raman spectra of the supports are in agreement with the XRD results (Fig. 1). Alumina was not active in Raman. The spectrum of Nb_2O_5 showed a sharp, intense band at 695 cm^{-1} assigned to the symmetric stretching mode of niobia polyhedra [21]. The higher wavenumber compared with amorphous niobia is characteristic of the ordered structure of the hexagonal phase [21]. The Nb_2O_5 spectrum also presents bands at 306 and 230 cm^{-1} characteristic of the bending mode of Nb–O–Nb bonds. The Nb_2O_5/Al_2O_3 support presented three broad bands at 912, 679, and 234 cm^{-1}. The most intense band at 912 cm^{-1} can be attributed to the symmetric stretching mode $\nu_s([\text{–O–Nb–O–}]_n)$ of polymerized polyhedra (monolayer-type

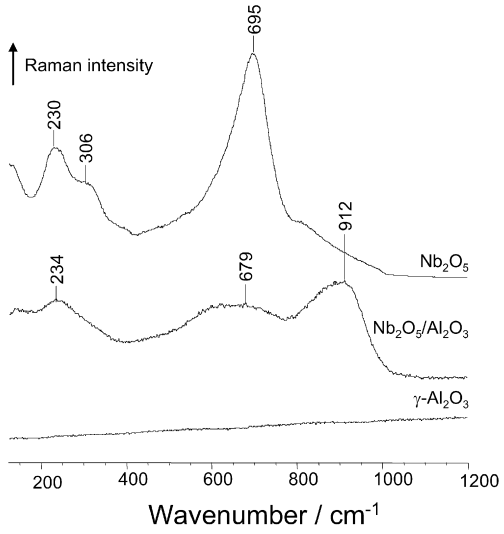

Fig. 1. Raman spectra of supports.

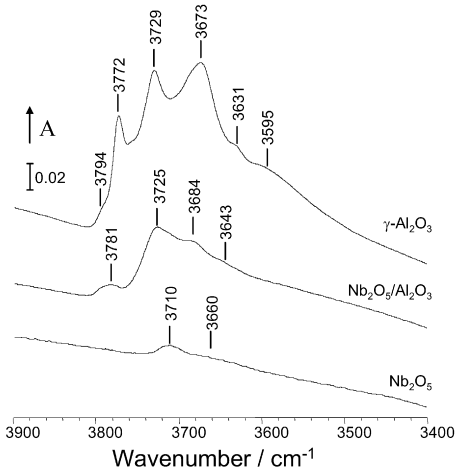

Fig. 2. FTIR spectra of supports in the OH region.

surface), whereas the band at around 680 cm^{-1} can be attributed to ν_s([–Nb–O–Nb–]$_n$) [18]. The band at 234 cm^{-1} is close to the value of 230 cm^{-1} observed for Nb_2O_5 and thus can be attributed to the bending mode of Nb–O–Nb bonds.

The characteristic band of the Nb=O stretching vibration expected at around 980 cm^{-1} was not observed on either Raman or IR spectra of the pure niobia (spectrum not shown), likely due to the low surface area of the oxide. For the Nb_2O_5/Al_2O_3 support, by difference between its IR spectra and that of alumina, a fundamental narrow band at around 995 cm^{-1} could be observed indicating the presence of mono oxo species at the support surface [18]. Thus, the IR and Raman results indicate the high dispersion of niobia as previously suggested by the BET and XRD results.

The IR spectra in the OH region of supports activated under vacuum are shown in Fig. 2. The complexity of the alumina spectrum, which is assigned to OH groups bound to aluminum atoms in different environments, can be seen [22]. In comparison, the spectrum of the niobium oxide is simple and presents a large and weak band with a maximum at 3710 cm^{-1} and a shoulder at 3660 cm^{-1}. Because the sample has a small surface area, the quantity of OH groups is smaller on the surface than on alumina.

In the spectrum of the Nb_2O_5/Al_2O_3 support, we can observe that alumina is partially covered; the same bands as for alumina alone are observed, but their intensity and the proportions between them are different than those of alumina alone. Basic hydroxyls, showing bands in the high wavenumber range, are preferentially consumed. The surface coverage of alumina can be estimated from the decrease of the OH region (not taking into account the increase due to Nb–OH); around 70% of the alumina surface is covered by niobia. Then we can conclude that the niobium is well dispersed on the surface of alumina. However, the presence of Nb–OH cannot be distinguished in the spectrum of Nb_2O_5/Al_2O_3. Adsorption of basic probe molecules was used to demonstrate the presence of such groups.

3.2. FTIR spectroscopy of basic probes adsorbed on the supports

Acidic properties of the pure supports were characterized by adsorption of basic probe molecules followed by IR spectroscopy. Figs. 3–5 show the spectra after adsorption on the supports of pyridine (Py), 2,6-dimethylpyridine (2,6-DMP) and CO, respectively. The main band characteristics of the probes adsorbed on Lewis acid sites (LAS) and Brønsted acid sites (BAS) of the supports are presented in Table 2. Pyridine is a commonly used probe for surface acidity characterization [23,24]. In the 1650–1400 cm^{-1} range, the position of two characteristic bands of Py ring vibration (ν_{8a} and ν_{19b}) serve as fingerprints of the presence of LAS and BAS on the surface. LAS sites are evidenced by a ν_{8a} band at around 1610 cm^{-1} and a ν_{19b} band at around 1450 cm^{-1}. Adsorption of Py on BAS leads to a ν_{8a} band at around 1630 cm^{-1} and to a ν_{19b} band at around 1545 cm^{-1}. Adsorption of 2,6-DMP leads to coordinated, protonated, and H-bonded species, and the IR spectra of the formed species allow differentiation among LAS, strongly acidic hydroxyl groups, and weakly acidic hydroxyl groups, respectively [25]. In particular, the ν_{8a} vibration, located at 1594 cm^{-1} in the spectrum of liquid 2,6-DMP, is very sensitive to the adsorption mode; a ν_{8a} wavenumber >1625 cm^{-1} characterizes protonated species (2,6-DMPH$^+$) whereas lower wavenumbers correspond to coordinated or H-bonded species [26,27]. The ν_{8b} band position at 1630 cm^{-1} is also characteristic of the formation of 2,6-DMPH$^+$ species. At low temperature, CO undergoes H-bond interactions with acidic hydroxyl groups, giving rise to OH...CO adducts. These interactions lead to a high-frequency shift of the ν(CO) stretching mode compared with the gas phase (2143 cm^{-1}) [28,29]. The stronger the BAS, the higher the wavenumber of the ν(CO/OH) mode. Interaction with LAS M^{n+} without d electrons leads to a ν(CO) mode at around 2200 cm^{-1}; the higher the wavenumber, the stronger the LAS site.

The infrared spectra of pyridine on alumina (Fig. 3) are in agreement with the literature values and show only the presence of LAS [25] also evidenced by 2,6-DMP and CO adsorption. In contrast, with 2,6-DMP and CO (which are more sensitive

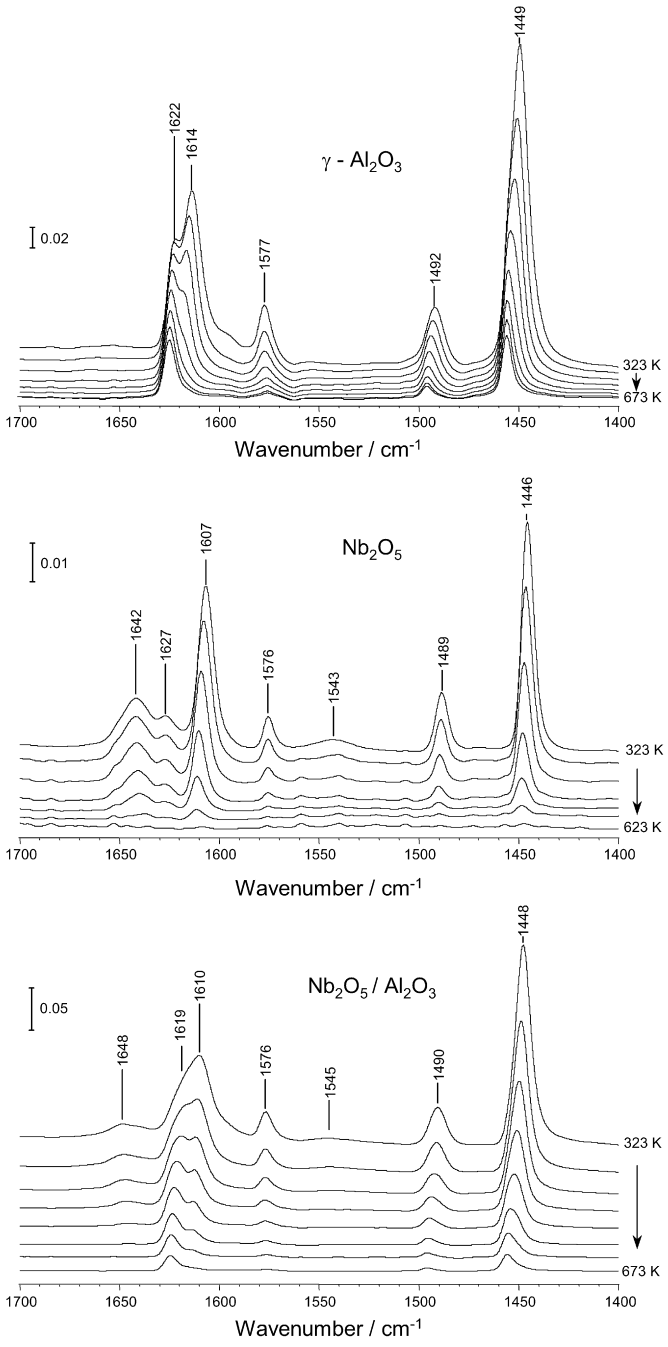

Fig. 3. FTIR spectra of 133 Pa of pyridine adsorbed on the supports and followed by evacuation at different temperatures.

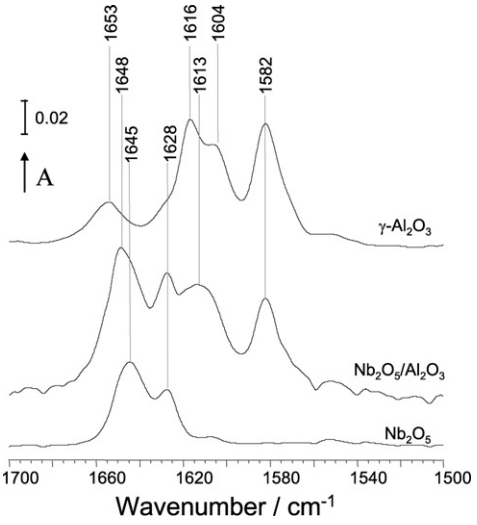

Fig. 4. FTIR spectra of 133 Pa of 2,6-dimethylpyridine adsorbed on the supports after evacuation at 323 K.

probes to weak BAS), such sites are revealed on alumina, in accordance with previous findings [25].

On Nb_2O_5, adsorption of Py, 2,6-DMP, and CO indicates the presence of LAS. These sites are weaker than those of alumina (Table 2). This is illustrated by the wavenumber and stability of the coordinated pyridine and 2,6-DMP species. As an example, after evacuation at high temperature (623 K), no pyridine (band at 1607 cm^{-1} in Fig. 3) remained adsorbed on the niobia surface, whereas even after evacuation at 673 K the band characteristic of Py on LAS at 1622 cm^{-1} remained on the alumina spectrum. The detection of a band at 1627 cm^{-1} after Py adsorption on Nb_2O_5 must be mentioned. Indeed, a band at such wavenumber could be assigned to either (i) the ν_{8a} vibration mode of pyridine coordinated to very strong Lewis acid sites or (ii) the ν_{8b} vibration mode of protonated pyridine. The elimination of the 1627 cm^{-1} band after thermodesorption at 573 K while that at 1607 cm^{-1} (which characterized weak LAS) remains present shows that this band is specific for pyridine interaction with BAS. Note that the absence of strong LAS on Nb_2O_5 explains the clear observation of this vibration mode. CO adsorption confirms the presence of weak LAS on Nb_2O_5, because the wavenumber associated with CO interacting with LAS is higher for alumina than for niobia (Table 2). The three probes also show the presence of acidic Nb–OH that are strong BAS because even after evacuation at 523 K, adsorbed pyridine on BAS can be observed (Fig. 3). The results obtained with CO adsorption also show that BAS of niobia are stronger than those of alumina, because the band characteristic of CO/OH is observed at higher wavenumber on niobia [ν(CO) = 2163 cm^{-1}] than on alumina [ν(CO) = 2153 cm^{-1}] (Fig. 5B).

The shift of the ν(OH) band due to CO interaction is also a tool for comparing the strength of BAS; the greater the shift, the stronger the site. Fig. 5A shows spectra obtained after the addition of small doses of CO on Nb_2O_5 in the ν(OH) and ν(CO) ranges. The shift of the ν(OH) band is evidenced by the decrease of the initial band and the increase of the band attributed to perturbed hydroxyls. The addition of small doses helps to differentiate hydroxyl groups with different Brønsted acid strengths in the same sample. In the case of niobia, two decreasing bands can be seen at 3719 and 3670 cm^{-1}. The band at 3719 cm^{-1} shows a positive–negative effect for the first doses of CO, indicating an indirect perturbation, likely due to CO coordinated on LAS located in the vicinity of OH groups. In contrast, at higher doses, the clear perturbation of the band at 3719 cm^{-1} gives rises to a new ν(OH) band at 3526 cm^{-1}. The band at 3670 cm^{-1} is perturbed by addition of the first doses of CO and gives rise to the band at lower wavenumber (around 3460 cm^{-1}). The variation in the ν(OH) due to the perturbation by CO [$\Delta\nu$(OH)] can be calculated based on these attributions.

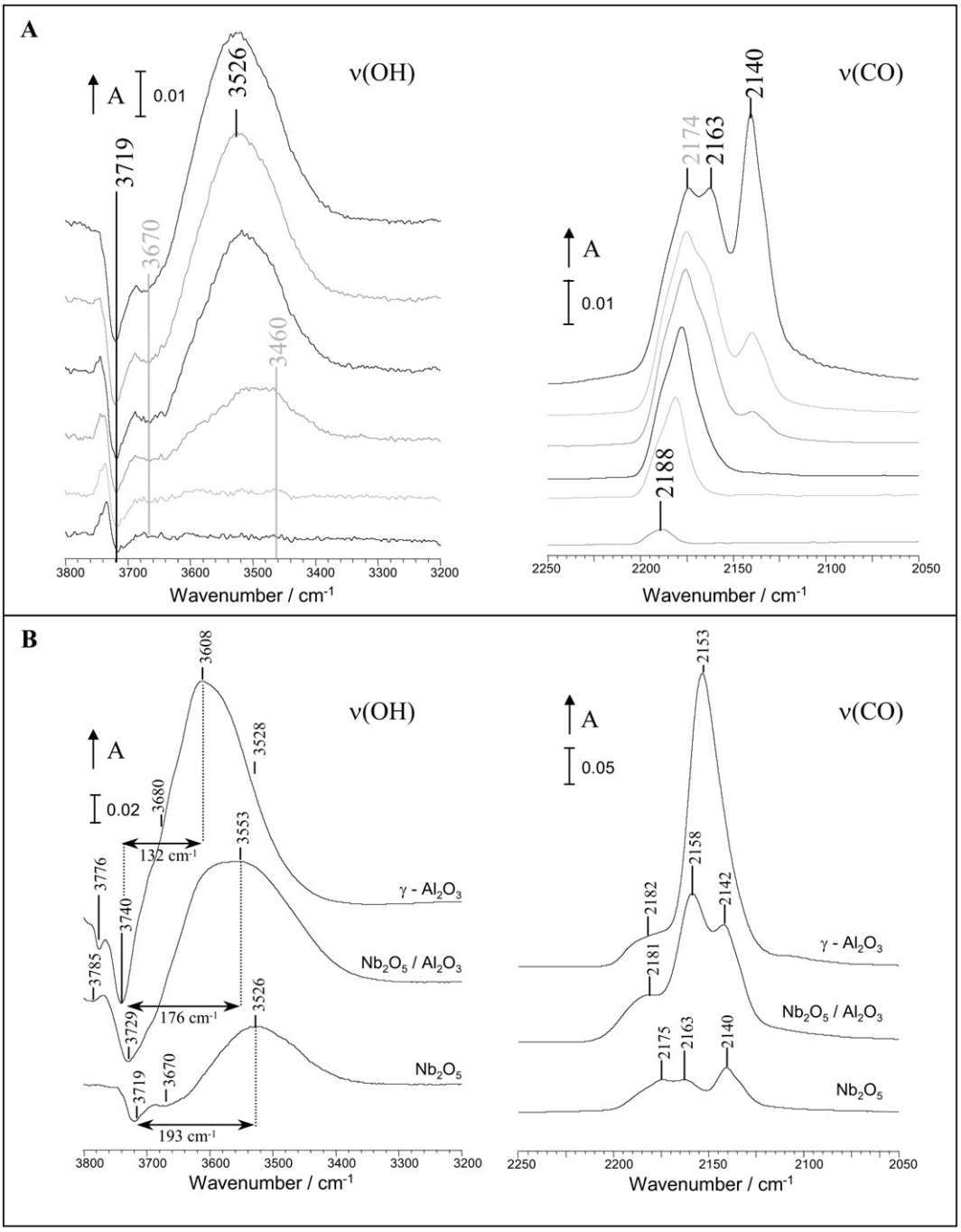

Fig. 5. (A) FTIR spectra of increasing doses of CO adsorbed at 100 K on Nb_2O_5. (B) Comparison of FTIR spectra of 133 Pa of CO adsorbed at 100 K on the supports.

The values of 210 and 193 cm^{-1} thus obtained demonstrate that the hydroxyl groups giving rise to the band at 3670 cm^{-1} are stronger BAS than those giving rise to the band at 3719 cm^{-1}. A $\Delta\nu$(OH) value of 193 cm^{-1}, associated with a ν(CO) of 2163 cm^{-1}, is in accordance with the previously reported correlation between the $\Delta\nu$(OH) and the ν(CO) band corresponding to a OH...CO adduct [30]. The position of the ν(CO) band for the second type of hydroxyl is somewhat hazardous, due to close proximity of the band characteristic of weak LAS.

The same study can be conducted for the other supports (Fig. 5B). The $\Delta\nu$(OH) increases with the niobia content in the support, confirming that BAS are stronger on niobia than on alumina.

The spectra obtained after adsorption of the three probes on Nb_2O_5/Al_2O_3 present bands characteristic of interaction with LAS as strong as on alumina. In the case of Py adsorption on Nb_2O_5/Al_2O_3, the massif attributed to the ν_{8a} stretching mode has at least two components as observed for alumina, indicating LAS of different strength. The shift toward lower wavenumbers of the ν_{8a} massif compared with alumina may be explained by preferential coverage of strong LAS of Al_2O_3 by niobium.

Table 2
Characteristic IR bands of basic probe molecules adsorbed on Lewis acid site (LAS) and Brønsted acid sites (BAS) for the three supports (value given for a probe pressure of 133 Pa)

Support	Pyridine				2,6-DMP		CO	
	LAS (cm^{-1})		BAS (cm^{-1})		LAS (cm^{-1})	BAS (cm^{-1})	LAS (cm^{-1})	BAS (cm^{-1})
	ν_{8a}	ν_{19b}	ν_{8a}	ν_{19b}	ν_{8a}, ν_{8b}	ν_{8a}, ν_{8b}	ν(CO)	ν(CO)
Al_2O_3	1622 1614	1449			1616, 1582	1653, 1628	2185	2153
Nb_2O_5	1607	1446	1642	1543	1603, 1582	1645, 1628	2174	2163
Nb_2O_5/Al_2O_3	1619 1610	1448	1648	1545	1613, 1582	1648, 1627	2181	2158

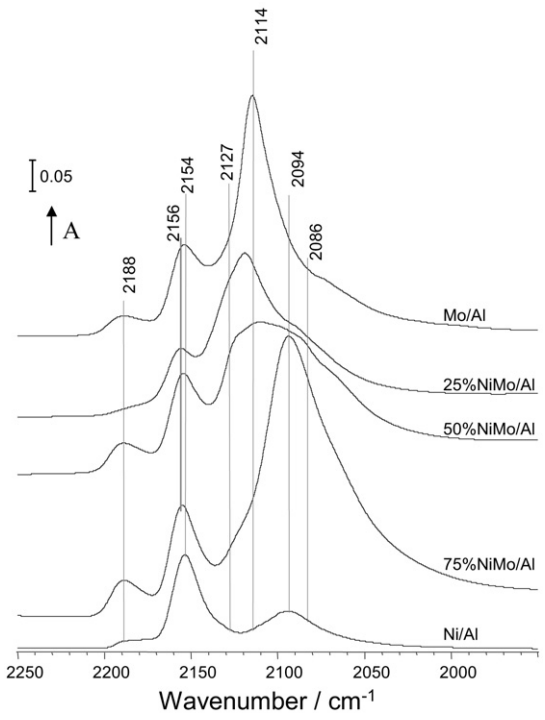

Fig. 6. Comparison of FTIR spectra of 133 Pa of CO adsorbed at 100 K on sulfided NiMo/Al catalysts.

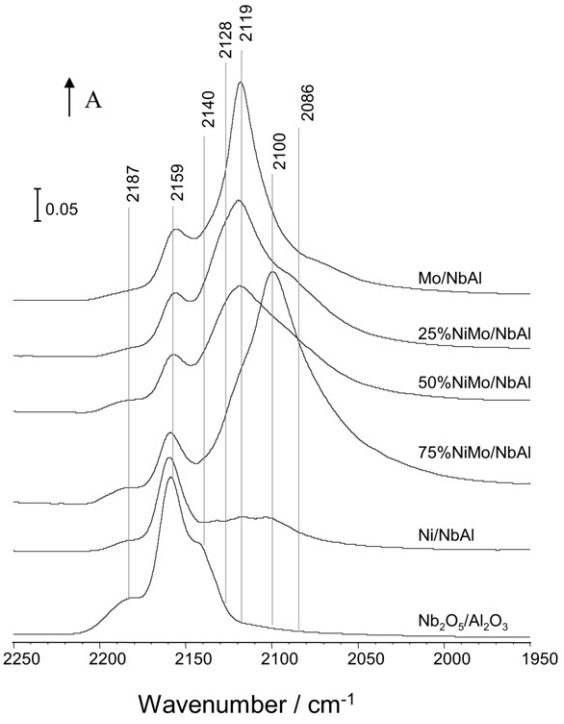

Fig. 7. Comparison of FTIR spectra of 133 Pa of CO adsorbed at 100 K on sulfided NiMo/NbAl catalysts.

For CO and 2,6-DMP adsorption on Nb_2O_5/Al_2O_3, the bands associated with BAS have wavenumbers in between those of alumina and niobia, indicating that these BAS are of intermediate strength compared with the pure supports. Indeed, according to the band position for the three probes (Table 2), BAS sites are weaker on Nb_2O_5/Al_2O_3 than on pure Nb_2O_5, but nonetheless these BAS are strong enough to protonate Py, in contrast to the BAS of Al_2O_3.

According to the Raman results, niobia supported on alumina formed polymerized polyhedra, as observed for a monolayer. A study by Jehng and Wachs [31] on similar system found that BAS could be due to slightly distorted surface niobium oxide octahedral, as well as NbO_7 and NbO_8, structures. LAS correspond to highly distorted surface NbO_6 octahedra sites.

Resuming the acid properties of the supports, alumina has strong LAS and weak BAS, niobia has weak LAS and strong BAS and niobia/alumina has intermediate LAS and BAS sites.

3.3. FTIR spectroscopy of adsorbed CO on sulfided catalysts

The sulfided NiMo catalysts were characterized by FTIR spectroscopy of adsorbed CO to investigate the nature and the amount of surface sites. The CO adsorption was performed at about 100 K, to increase the coverage of the probe molecule on weak sites such as the OH groups of the support and the sites of the metal phase. The sulfided catalysts deposited on pure niobia are not sufficiently transparent to the IR beam to allow transmittance analysis of self-supported wafers.

Figs. 6 and 7 compare the spectra of CO adsorbed on the sulfided NiMo catalysts supported on pure alumina and on niobia/alumina, respectively, for adsorption of 133 Pa of CO at equilibrium. Fig. 8 shows the spectra obtained after adsorption of increasing small doses of CO on the sulfided 25% and 50% NiMo catalyst supported on alumina and niobia/alumina.

Figs. 6 and 7 show that the presence of niobium in the catalysts induces an increase of the acid strength of the OH

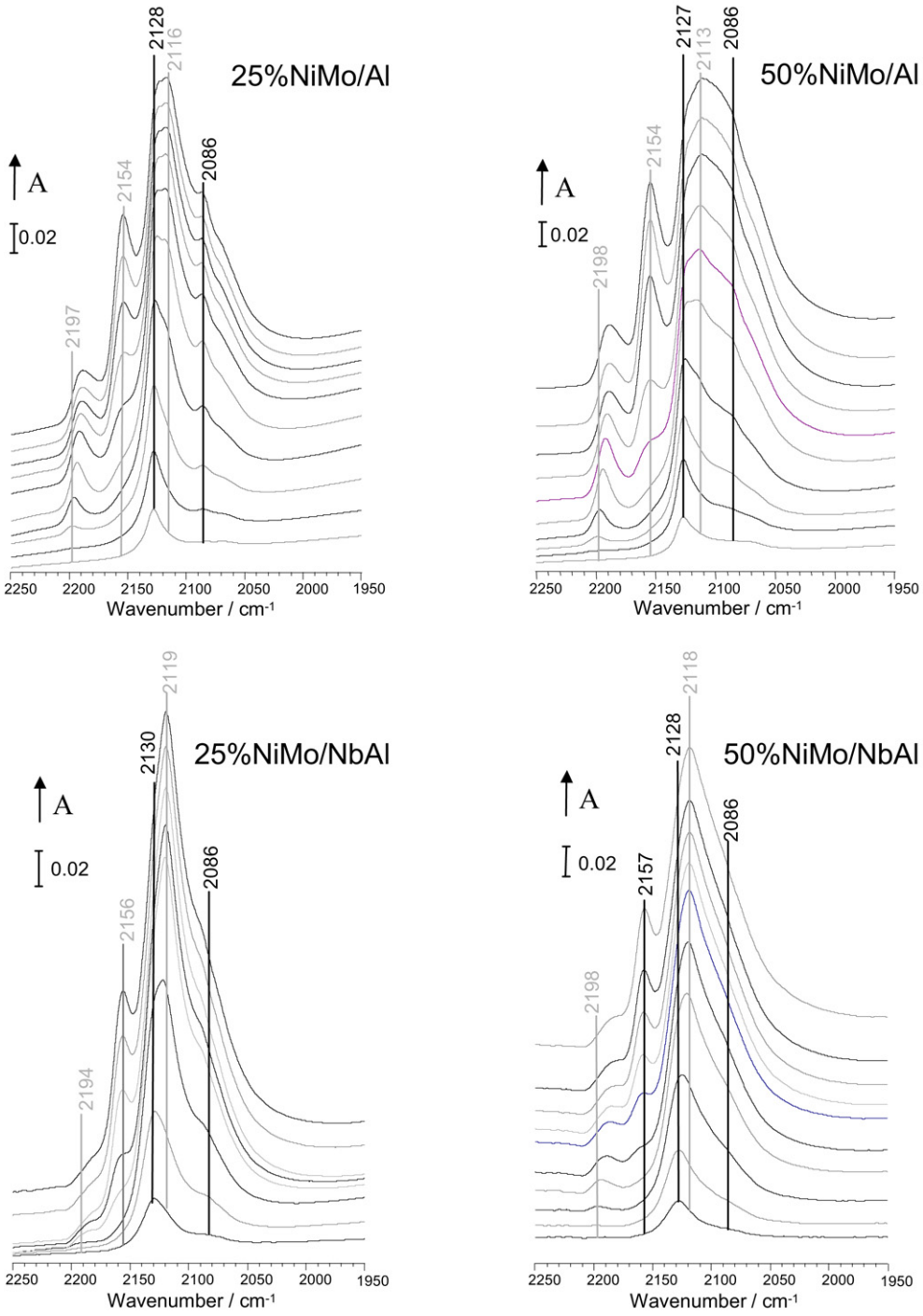

Fig. 8. FTIR spectra of increasing doses of CO adsorbed at 100 K on sulfided catalysts.

groups of the support. Indeed, on supported NiMo catalysts, the CO/OH band is observed at higher wavenumbers on NiMo/NbAl [ν(CO) = 2159 cm^{-1}] than on NiMo/Al [ν(CO = 2154 cm^{-1}]. This result is in agreement with previous findings of studies performed on supports alone. On alumina, a shift of the CO/OH band toward the high wavenumbers is observed going from the pure Ni to the pure Mo catalysts. This shift indicates an increasing acidity of hydroxyl groups going from Ni to Mo catalysts. The origin of this strengthening is not straightforward; interaction between sulfide SH groups and support OH can be proposed. There is also an effect of CO coverage, because the shift is not observed for small doses (Fig. 8).

The interactions of CO with the sulfide phases are characterized by the presence of bands in the 2130–2080 cm^{-1} range (Table 3). Regarding the spectrum of Mo/Al (Fig. 6), the band at 2114 cm^{-1} is attributed to CO interacting on molybdenum sulfide, in agreement with previous studies [17,32]. From the spectra of nickel-rich catalysts, 75% NiMo/Al and Ni/Al, the band at 2094 cm^{-1} can be attributed to CO interacting with nickel sulfide sites [33]. As shown in Figs. 6 and 7, the interac-

Table 3
Characteristic IR bands (cm^{-1}) of CO adsorbed on the metallic phase supported on alumina and niobia/alumina supports

Support	Mo	NiMo	Ni
Al_2O_3	2114	2127–2086	2094
Nb_2O_5/Al_2O_3	2119	2128–2086	2100
$\Delta\nu$(CO)[a]	+5	0	+6

[a] Variation of the ν(CO) band position going from the Al_2O_3 support to the Nb_2O_5/Al_2O_3 support.

tion of CO with NiMo phase gives rise to a complex massif that contains different bands. Analysis of the spectra corresponding to adsorption of increasing doses allows discrimination of the various components of this massif (Fig. 8). Thus, in the spectrum of CO adsorbed on 25% NiMo/Al, a broad band with two maxima around 2116 and 2128 cm^{-1} and a shoulder around 2086 cm^{-1} can be seen. Adsorption of CO on the 50% NiMo/Al catalysts also leads to a wide band with at least three components, whereas the shoulder at around 2086 cm^{-1} is more intense than that on 25% NiMo/Al. Thus, the two bands at around 2128 and 2086 cm^{-1}, which are not present on unicomponent catalysts, are attributed to the NiMoS phase, in accordance with previous findings [32–34]. On 50% NiMo/Al, the greater intensity of the band at 2086 cm^{-1} suggests a higher amount of mixed phase on this catalyst. Nevertheless, the detection of a signal at about 2116 cm^{-1} shows that not all of the sulfide phase is promoted on these two catalysts.

Fig. 7 shows that the pure Mo sulfide phase supported on NbAl is characterized by a band at 2119 cm^{-1}, whereas the Ni sulfide phase on this support is characterized by a band at 2100 cm^{-1} (as deduced from analysis of the spectra for Ni/NbAl and 75% NiMo/NbAl). Comparing these wavenumbers with those reported for Mo/Al and Ni/Al shows that on NbAl-supported catalysts, the frequency of CO interacting with these two sulfide phases is shifted toward higher values ($\sim +5$ cm^{-1}) (Table 3).

As can be seen in Figs. 7 and 8, interaction of CO with NiMo catalysts supported on NbAl gives rise to a main band at $\sim$2118 cm^{-1}. This demonstrates that unpromoted Mo sites are predominant on 25% and 50% NiMo/NbAl. However, analysis of the spectrum corresponding to the first CO doses provides evidence of a band at $\sim$2128 cm^{-1}, demonstrating the formation of NiMoS mixed phase. Note that this band is present only as a weak shoulder on the spectrum corresponding to a CO adsorption of 133 Pa, indicating that only a weak fraction of the sulfide phase sites corresponds to the mixed NiMoS phase. In parallel, the shoulder observed at $\sim$2086 cm^{-1} on alumina-supported catalysts is only slightly visible on the spectra of the 25% and 50% NiMo/NbAl; this confirms the previous observation. In addition, note that although the bands attributed to the NiMoS phase are weak on the niobia–alumina support, clearly no shift due to the support can be seen, in contrast with what was observed for the single metal catalysts (Table 3).

Finally, note that the band at 2135 cm^{-1} seen in the case of Mo/NbAl that we have attributed to NbS_x [17] cannot be distinguished on the spectra of sulfided 25% and 50% NiMo catalyst supported on NbAl (Fig. 8). Thus, formation of NbS_x species is not evidenced by the IR study.

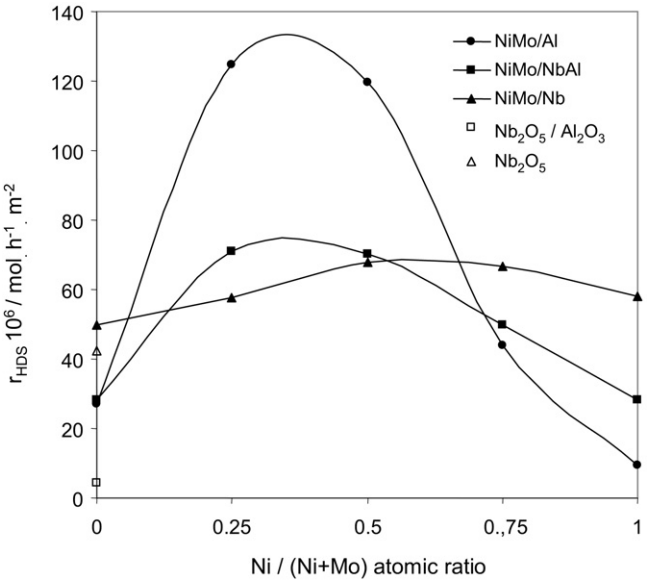

Fig. 9. Thiophene HDS activity of NiMo catalysts and supports.

3.4. Thiophene hydrodesulfurization activity

Supported NiMo catalysts and supports alone were evaluated in thiophene HDS. Because the catalysts have considerably different surface areas, Fig. 9 presents the rate per square meter of catalyst. The activities of pure supports are represented by open symbols. As reported previously [2,4,15], alumina-supported NiMo mixed sulfides are more active than the pure nickel and molybdenum sulfides. This activity pattern results from the synergy between nickel and molybdenum in contact with each other on an adequate support, after sulfidation. In agreement with previous results, activity is maximum for the 25% and 50% NiMo/Al catalysts. This suggests that the NiMoS phase is present in higher amounts in these latter catalysts.

Activity was lower for the niobia/alumina and niobia-supported catalysts with the same NiMo content compared with the catalysts deposited on alumina. Thus, it can be deduced that niobia hinders the formation of the NiMoS phase, giving rise to the synergetic effect.

Another interesting observation is that the addition of niobia increases the activity of pure nickel catalysts. Thus, the activity of Ni on pure niobia is even greater than that of the corresponding Mo catalyst. However, on the niobium catalyst series, the contribution of niobium to the catalyst activity is noticeable. Indeed, previous studies showed that niobium is partially sulfided, and niobium sulfide has significant activity [15,17]. Thus, to better estimate the activity of the NiMo sulfide phase for HDS of thiophene, support activities were subtracted from catalyst activities. Table 4 presents these results for all materials. Column 1 presents the same results as for Fig. 9, that is HDS activity of the catalysts per square meter; column 2 presents the catalyst activity minus the support activity; and column 3 presents the results of column 2 per total metal content. We

Table 4
Thiophene HDS activity of NiMo catalysts and supports

Catalyst	r_{HDS} (10^{-6} mol h^{-1} m^{-2})	Difference of activity[a] (10^{-6} mol h^{-1} m^{-2})	Difference of activity[b] (mol_{th} mol^{-1}_{metal} h^{-1})
Al_2O_3	0.0	–	
Mo/Al	27.0	27.0	3.51
25% NiMo/Al	124.6	124.6	15.52
50% NiMo/Al	119.5	119.5	15.82
75% NiMo/Al	43.9	43.9	5.77
Ni/Al	9.5	9.5	1.15
Nb_2O_5/Al_2O_3	4.4	–	
Mo/NbAl	28.3	23.9	2.55
25% NiMo/NbAl	70.8	66.4	7.31
50% NiMo/NbAl	70.1	65.6	7.52
75% NiMo/NbAl	50.0	45.6	5.42
Ni/NbAl	28.3	23.9	2.82
Nb_2O_5	42.3	–	
Mo/Nb	50.0	7.7	1.00
25% NiMo/Nb	57.7	15.4	1.93
50% NiMo/Nb	68.0	25.7	3.11
75% NiMo/Nb	66.7	24.4	3.20
Ni/Nb	58.1	15.8	2.39

[a] Difference of activity: $r_{(catalyst)} - r_{(support)}$ in 10^{-6} mol h^{-1} m^{-2}.

[b] Difference of activity per mole of metal (Ni + Mo) in $mol_{thiophene}$ mol^{-1}_{metal} h^{-1}.

should consider that this calculation underestimates the contribution of metal phases, because the supports in the catalysts are partially covered by the metals. In contrast, the support activity can be modified by the presence of metal. Indeed, in the case of niobium, sulfidation is known to increase in the presence of metal, and niobium sulfide is known to be active in HDS [15,17].

Based on the catalyst activity (column 1), molybdenum on niobia is twice as active as Mo/Al and Mo/NbAl, but the significant contribution of niobia to catalyst activity is responsible for this superior activity, and in fact the activity per Mo atom decreases with increasing niobium content (column 3).

Regarding the Ni catalysts, niobium-containing supports increase nickel sulfide activity per metal atom. Ni/Nb and Ni/NbAl catalysts are approximately two times more active than Ni/Al (column 3).

Comparing the results in the last column for the NiMo catalysts shows that the synergetic effect between nickel and molybdenum is maximum on alumina (25% and 50% NiMo/Al). However, the higher activities of 25% and 50% NiMo/NbAl compared with those of the corresponding monometallic catalysts indicate that this effect is present in these catalysts as well. On niobia, the synergetic effect appears for the 50% and 75% NiMo/Nb, but it remains very low.

In conclusion, the synergetic effect of nickel and molybdenum for thiophene HDS decreases with increasing niobia content in the support.

3.5. 2,6-Dimethylaniline (2,6-DMA) hydrodenitrogenation activity

In previous work, it has been proposed that HDN of alkylanilines over NiMo catalysts can generate three types of products: (i) aromatic hydrocarbons denitrogenated via direct ammonia elimination (DDN), (ii) saturated hydrocarbons denitrogenated via hydrogenation followed by elimination (HYG + HYD); and (iii) nitrogen-containing products formed by disproportionation (DIS) [19]. The first route is very interesting, because the denitrogenation occurs with low hydrogen consumption (Scheme 1). From 2,6-DMA, it leads to xylene formation, which also occurs to some extent via the hydrogenation route (HYG). In what follow, XYL represents the sum DDN + HYG. The three routes XYL, HYD, and DIS are strictly parallel [19].

Previously, we found that niobium increased the selectivity of molybdenum sulfide to xylene production in 2,6-dimethylaniline HDN [17]. For the three routes, sulfided niobia presented significant activity, whereas pure alumina was inactive.

In the present work, we compared the activity of pure nickel (Ni/supports), pure molybdenum (Mo/supports), and 25% NiMo/supports sulfided catalysts in 2,6-dimethylaniline HDN. We also evaluated the supports alone.

3.5.1. Activity in the presence of H_2S

Table 5 reports the rate for each reaction route: HYD, XYL and DIS in presence of H_2S. In the same manner as for thiophene HDS, to estimate the activity of the supported phase the activity of the support alone is subtracted from the catalyst activity (columns 5–7).

First, we can observe the effect of the support on monometallic catalysts. As reported previously, molybdenum on niobia and niobia/alumina are very active for xylene production compared with molybdenum on alumina. The activity of pure molybdenum catalyst for the DIS route also increases with the niobium content in the support, whereas the activity for HYD is modified only slightly by the nature of the support (activity by metal atom shows a slight decrease with increasing niobium content). Thus, the selectivity of Mo catalysts for the XYL is

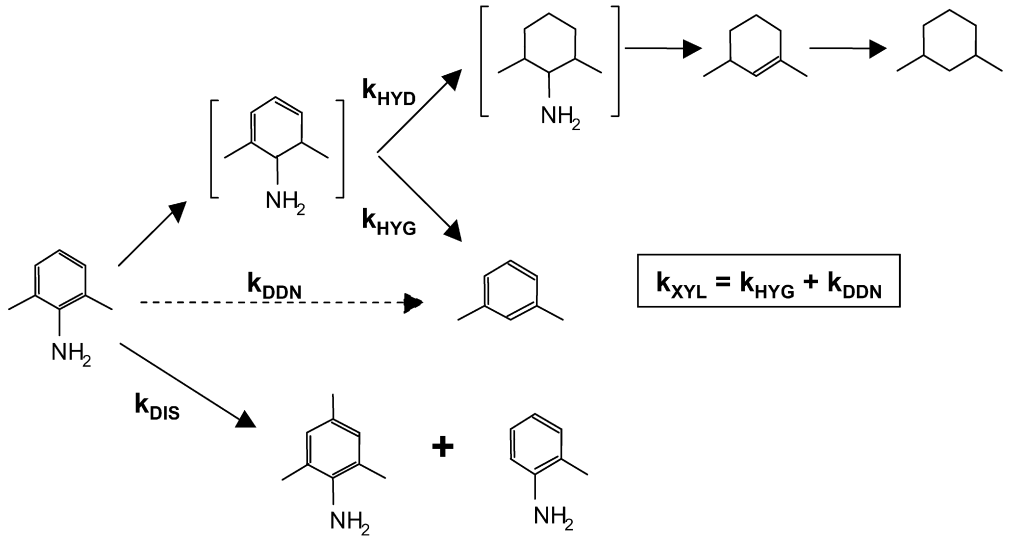

Scheme 1. Reaction network of 2,6-dimethylaniline decomposition.

Table 5
Activity of NiMo catalysts and supports in decomposition of 2,6-dimethylaniline in presence of H_2S

Catalyst	Activity (10^{-6} mol h^{-1} m^{-2})			Difference of activity (mol_{DMA} mol^{-1}_{metal} h^{-1})		
	r_{HYD}	r_{XYL}	r_{DIS}	r_{HYD}	r_{XYL}	r_{DIS}
Al_2O_3	0	0	0	–	–	–
Mo/Al	5.03	0.85	1.14	0.65	0.11	0.15
25% NiMo/Al	5.89	0.36	1.05	0.73	0.04	0.13
Ni/Al	0.88	0.05	0.13	0.11	0.01	0.02
Nb_2O_5/Al_2O_3	0.17	0.05	0.14	–	–	–
Mo/NbAl	5.47	7.23	2.22	0.56	0.77	0.22
25% NiMo/NbAl	6.89	1.15	1.60	0.74	0.12	0.16
Ni/NbAl	2.00	0.25	0.43	0.22	0.02	0.03
Nb_2O_5	2.16	0.64	1.58	–	–	–
Mo/Nb	5.38	10.97	3.64	0.42	1.34	0.27
25% NiMo/Nb	5.30	3.40	3.04	0.39	0.35	0.18
Ni/Nb	5.67	1.54	2.82	0.53	0.14	0.19

greatly improved on the niobium-containing support at the expense of the HYD route. For nickel catalysts, the activity for the three routes increases with increasing niobium content on the support, but the selectivity for HYD remains the greatest for the three supports, in contrast with the case of Mo catalysts. Comparison between the two metals shows that for the three routes, Mo is more active than Ni. Only on pure niobia support is the hydrogenation activity of pure nickel catalyst comparable to that of pure Mo catalyst. The greater hydrogenation activity of Ni/Nb compared with Ni/Al is in accordance with the greater activity for HDS of thiophene observed in the present study and reported previously [15]. This greater activity of Ni catalyst when supported on niobia compared with that supported on alumina was attributed to an increase in the nickel present on niobia surface, as demonstrated by XPS data [15], due to either an absence of Ni loss in the support or the formation of smaller Ni_2S_3 particles compared with alumina.

Regarding the bimetallic catalysts, we found that 25% and 25% NiMo/NbAl are more active for the HYD route than the respective monometallic catalysts, demonstrating a synergetic effect between the two metals. The hydrogenation activity of the 25% NiMo catalyst on niobia/alumina is greater than that on alumina, but the activity per metal content without the support contribution is the same in the two catalysts. A synergetic effect between Ni and Mo for the HYD route is not observed on pure niobia catalysts. However, the HYD activity of 25% NiMo/Nb is significant and can be related to the stronger activity of pure nickel on this support compared with other supports.

For the xylene route, the activity of NiMo catalysts increases with increasing niobium content. However, on pure niobia, the activity for XYL is much lower for the 25% NiMo than for the pure molybdenum. We previously proposed that this special activity of the molybdenum and niobium sulfide catalysts would be a result of a synergy between the Mo sulfide phase and the Nb sulfide (or oxysulfide), responsible for the C–N bond cleavage [17]. Apparently, the addition of nickel inhibits this effect.

For the disproportionation route, the activity of 25% NiMo catalysts increases with increasing niobium content in the support, as was seen for monometallic catalysts. No synergetic effect between Mo and Ni was observed for this route, whatever the support.

3.5.2. *Effect of the absence of H_2S in the reaction mixture*

Table 6 reports the HDN activities of all supports and catalysts in the absence of H_2S. As in the presence of H_2S, alumina is inactive. The two niobium-based supports exhibit only a slight decrease in activity in all routes in the absence of H_2S compared with the experiments carried out in the presence of H_2S. The hydrogenation activity of pure molybdenum catalysts is only slightly modified by the absence of H_2S. For the disproportionation route, a moderate decrease in activity can be seen. In contrast, the xylene formation on pure molybdenum catalysts is significantly greater without H_2S on the three supports, with this effect relatively more pronounced on alumina (Fig. 10).

The activities of pure nickel catalysts (per metal atom) on all supports are similar with and without H_2S for the three routes.

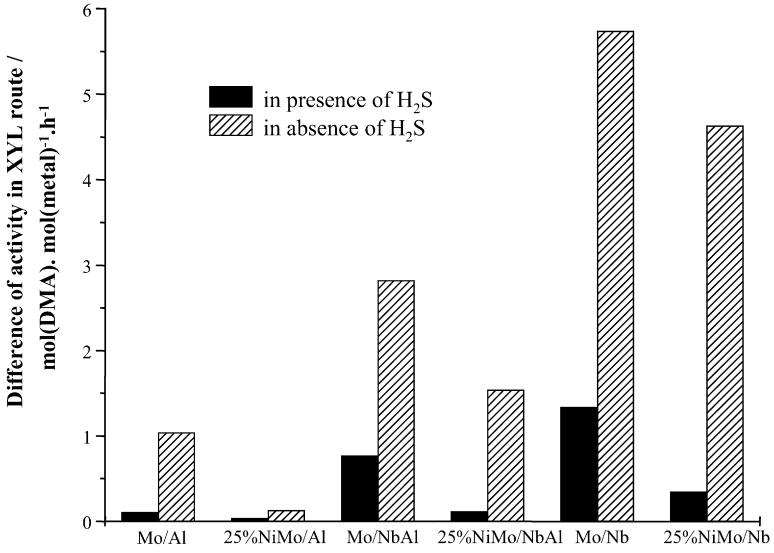

Fig. 10. 2,6-Dimethylaniline HDN: activity in xylene formation route per metal content of molybdenum based catalysts, in presence and absence of H_2S.

Table 6
Activity of NiMo catalysts and supports in decomposition of 2,6-dimethylaniline in absence of H_2S

Catalyst	Activity (10^{-6} mol h^{-1} m^{-2})			Difference of activity (mol(DMA) mol(metal)$^{-1}$ h^{-1})		
	rHYD	rXYL	rDIS	rHYD	rXYL	rDIS
Al_2O_3	0	0	0	–	–	–
Mo/Al	5.63	7.99	0.49	0.73	1.04	0.06
25% NiMo/Al	11.87	1.05	0.18	1.48	0.13	0.02
Ni/Al	0.40	0.01	0.04	0.05	0.00	0.01
Nb_2O_5/Al_2O_3	0.11	0.05	0.08	–	–	–
Mo/NbAl	5.32	26.49	1.08	0.56	2.82	0.11
25% NiMo/NbAl	10.83	14.03	0.63	1.18	1.54	0.06
Ni/NbAl	2.93	0.22	0.16	0.33	0.02	0.01
Nb_2O_5	1.60	0.68	1.21	–	–	–
Mo/Nb	4.94	44.96	2.73	0.43	5.74	0.20
25% NiMo/Nb	5.78	37.60	2.61	0.52	4.63	0.18
Ni/Nb	4.59	1.31	2.18	0.45	0.10	0.15

As observed for pure molybdenum catalysts, the activity of 25% NiMo catalysts in disproportionation route decreases without H_2S, whereas the xylene formation markedly increases. For HYD, activity increases in absence of H_2S, and the synergetic effect between Ni and Mo can be seen on the three supports in this case.

4. Discussion

Our findings clearly demonstrate the effect of the support nature on the HDS activity of NiMo catalysts. The synergy effect of Ni and Mo is much lower on niobia-containing supports than on alumina, in accordance with the findings of Faro and dos Santos [15]. In all likelihood, nickel and molybdenum interact preferentially with niobium compared with each other, inhibiting the formation of the NiMoS phase. The CO FTIR results are in agreement with this hypothesis; the band at 2128 cm^{-1} and the shoulder at 2086 cm^{-1} which may be attributed to CO adsorbed on the NiMo sulfide sites, are more intense for the most active catalysts. Strong interaction of pure metal with niobia is also evidenced by the CO results; compared with alumina-supported catalysts, on niobia–alumina, the ν(CO) band of CO in interaction with the metal is blue-shifted. Thus, the absence of shift of the ν(CO) band of CO in interaction with the NiMoS phase when the support is niobia–alumina instead of alumina suggests that the NiMoS phase is supported on the part of alumina not covered by niobia.

The higher activities of 25% NiMo/Al and 25% NiMo/NbAl catalysts for hydrogenation of 2,6-DMA compared with monometallic catalysts are in agreement with the HDS results and reveal the synergetic effect between the two metals. This comparable behavior suggests that the active sites for hydrogenation of nitrogenated compound are also the active sites for HDS, that is, the NiMo sulfide. For this HYD route, the effect of the presence of H_2S is moderate. However, it can be seen that the synergy effect between Ni and Mo is stronger in absence of H_2S. This can be explained by a change in the reaction mechanism as proposed by van Gestel et al. [35]. In the absence of H_2S in the flow, hydrogenation occurs after heterolytic dissociation of H_2. In the presence of H_2S in the flow, H_2S can act as a poison for the site of dissociation of H_2 or can be dissociated to SH^- and H^+ species and thus lead to hydrogenation.

Disproportionation reactions are typically catalyzed by BAS. The high activities of niobium-based catalysts for this route are in agreement with our IR characterization results obtained by pyridine, 2,6-DMP, and CO. Indeed, niobia and niobia/alumina present strong BAS, whereas alumina has only weak BAS. Thus, we propose that the BAS related to niobia are responsible for the high disproportionation activities of niobium-based catalysts.

The disproportionation trend for monometallic catalysts indicates that molybdenum sulfide is more active than nickel sulfide. This result is in accordance with previous results of van Gestel et al. verifying that H_2S dissociation is involved in the generation of surface acidity on $Mo(Co)/Al_2O_3$ catalysts [19]. Their study showed that such H_2S dissociation could be re-

sponsible for protonation of 2,6-DMA molecule, leading to an intermediate species for the disproportionation reaction. In contrast, Ni has been shown to inhibit the activity of Mo/Al_2O_3 even in the presence of H_2S, and thus H_2S dissociation is hindered on Ni sites [35]. Thus, the higher activity of Mo catalysts compared with Ni catalysts can be explained by the former's ability to dissociate H_2S. This ability can be linked with the strength of metal LAS demonstrated by the IR results. The frequency of CO adsorbed on sulfided molybdenum is higher than that of CO adsorbed on sulfided nickel, indicating that MoS_x is a stronger LAS than NiS_x. Strong LAS could be responsible for H_2S dissociation on Mo catalysts.

Alternatively, we can propose a strengthening of the OH BAS with Mo. Indeed, on Al_2O_3, a slight blue shift of the band characteristic of CO/(OH) going from pure Ni to pure Mo can be seen in Fig. 6. However, the involvement of H_2S dissociation in the DIS mechanism is supported by the fact that the presence of H_2S in the reaction medium favors the DIS route. The effect is more pronounced for catalysts supported on alumina, which has on its own the weaker BAS.

As mentioned previously, the DDN route leading to xylene formation is a particularly interesting route for denitrogenation, because it involves less hydrogen consumption than other routes. The proposed mechanism for DDN implies a C–N bond rupture on unpromoted molybdenum sulfide sites. Accordingly, pure molybdenum catalysts are the most active for this route. The Mo sites involved in the DDN route are described as highly unsaturated edge sites that can be easily poisoned by H_2S. This hypothesis is in concordance with our results, because activities for DDN increase significantly without H_2S for all Mo-containing catalysts. However, it must be pointed out that when supported on niobia-containing supports, pure nickel catalyst appears slightly active for XYL formation. Because pure niobia is itself active for the XYL route, we attribute the apparent activity of Ni catalysts supported on niobia or niobia/alumina to enhanced niobia activity rather than to nickel activity.

In contrast, in any case, the activity of support alone for XYL formation is much lower than that of the molybdenum-containing catalyst. However, the nature of the support has a significant effect on the catalyst activity for XYL formation. Xylene formation is greatest on niobia-supported catalysts in both the absence and presence of H_2S. Because the electronic properties of pure metal sulfides are modified on niobia, as revealed by the shift of the IR band associated with CO in interaction with supported metal LAS, we propose that the strong activity for XYL formation on niobia-supported catalyst is linked to this phenomenon. Comparing the favorable effect of niobia support for the XYL route with the decreased synergy effect on niobia-supported catalyst for HDS and HYD routes, we can infer that both metals interact preferentially with niobium than with each other.

Another interesting result for the XYL route is the effect of promotion of Mo by Ni versus the support nature. Indeed, on alumina, the XYL activity is divided by 8 when going from Mo to 25% NiMo. In this support, we can suppose that the decrease in activity for the XYL route is due to two phenomena: the lower amount of molybdenum and the promoting effect of Mo by Ni, which inhibits Mo activity for DDN [19]. The first factor should decrease the activity of the 25% NiMo/Al to 75% of the activity of the Mo/Al [expected activity, 0.78 mol(2,6-DMA) $\text{mol(metal)}^{-1}\,\text{h}^{-1}$]. The promotion of Mo by Ni explains the lower observed activity, which corresponds to only around 17% of the expected activity. On niobia-supported catalysts, the decrease in the XYL route is much lower when going from Mo to 25% NiMo; the activity decreases by a factor of 1.25. This activity decrease is the same order of magnitude as the decrease in Mo content. In this case, intrinsic activity of molybdenum is not affected by nickel. Accordingly, we have demonstrated the low promotion of Mo by Ni on this support for the HYD route of 2,6-DMA and for thiophene HDS. For Nb_2O_5–Al_2O_3, as for Al_2O_3, we can suppose that the decrease in activity for the XYL route is due to the lower amount of molybdenum and to the promoting effect of Mo by Ni on alumina not covered by niobia. The first cause should decrease the activity of the 25% NiMo/NbAl to 75% of the activity of the Mo/NbAl [expected activity, 2.11 mol(2,6-DMA) $\text{mol(metal)}^{-1}\,\text{h}^{-1}$]. The interesting point is that we can estimate the repartition of molybdenum on alumina not covered by niobia and on niobia. Indeed, on alumina, we can speculate that the promotion of Mo by Ni induces a reduction of activity of 83%, whereas no further decrease of activity is expected on niobia, because no promotion is expected. By this method, we obtain that 67% of Mo is on niobia and 33% is on alumina, and thus that the repartition of Mo is homogeneous on all the surface of the support, because 70% alumina coverage by niobia has been estimated by IR. Accordingly, for the monometallic Mo catalysts, the activity of the Mo/NbAl is near the sum of 67% of the activity of Mo/Nb and 33% of the activity of Mo/Al. The coherence of these calculations validates the previously mentioned hypothesis that the promoted phase NiMo is formed only on alumina not covered by niobia.

5. Conclusion

The present study has shown that using niobia as support, the activity of NiMo catalysts in thiophene HDS and in HDN of 2,6-DMA is no longer promoted by the synergy between Ni and Mo. The lack of synergy between molybdenum and nickel on niobia is explained by the strong interaction of each metal with niobia at the expense of interaction with each other. Nevertheless, niobia is an interesting support for the HDN of 2,6-DMA because it favors the XYL route, a way to remove nitrogen with low H_2 consumption. The activity for the XYL route on niobia is linked to the electron-deficient character of the Mo sulfide site, as revealed by CO adsorption followed by IR.

Therefore, using niobia/alumina as a support is a good compromise. Indeed, this study shows that on this support, the NiMoS phase is formed on the fraction of alumina not covered by niobia, whereas the molybdenum sulfide phase is located on the niobia. Consequently, compared with conventional NiMo supported on alumina, catalysts supported on niobia/alumina demonstrate acceptable HDS and HYD properties, along with high activity for direct denitrogenation.

Acknowledgments

The CNRS supported this work through the International Program for Scientific Cooperation with South America (project "Hydrotraitement et Développement Durable"); PETROBRAS also provided partial financial support. The authors thank Guillaume Clet for the Raman characterization, Valérie Ruaux and Wenbin Chen for their technical support, and the NUCAT/UFRJ for the XRD measurements.

References

[1] L. Zhang, G. Karakas, U.S. Ozkan, J. Catal. 178 (1998) 457.
[2] B.M. Vogelaar, P. Steiner, A.D. van Langeveld, S. Eijsbouts, J.A. Moulijn, Appl. Catal. A 251 (2003) 85.
[3] S.H. Yang, C.N. Satterfield, J. Catal. 81 (2003) 168.
[4] P. Baeza, M.S. Ureta-Zañartu, N. Escalona, J. Ojeda, F.J. Gil-Llambías, B. Delmon, Appl. Catal. A 274 (2004) 303.
[5] D. Zuo, M. Vrinat, H. Nie, F. Maugé, Y. Shi, M. Lacroix, D. Li, Catal. Today 93–95 (2004) 751.
[6] C. Dujardin, M.A. Lélias, J. van Gestel, A. Travert, J.C. Duchet, F. Maugé, Appl. Catal. A 322 (2007) 46.
[7] M. Breysse, P. Afanasiev, C. Geantet, M. Vrinat, Catal. Today 86 (2003) 5.
[8] L. Qu, M. Flechsenhar, R. Prins, J. Catal. 217 (2003) 284.
[9] D. Ferdous, A.K. Dalai, J. Adjaye, Fuel 85 (2006) 1286.
[10] F. Dumeignil, K. Sato, M. Imamura, N. Matsubayashi, E. Payen, H. Shimada, Appl. Catal. A 287 (2006) 135.
[11] M. Ziolek, Catal. Today 78 (2003) 47.
[12] M.A. Abdel-Rehim, A.C.B. dos Santos, V.L.L. Camorim, A.C. Faro Jr., Appl. Catal. A 305 (2006) 211.
[13] J.G. Weissman, Catal. Today 28 (1996) 159.
[14] V. Gaborit, N. Allali, C. Geantet, M. Breysse, M. Vrinat, M. Danot, Catal. Today 57 (2000) 267.
[15] A.C. Faro Jr., A.C.B. dos Santos, Catal. Today 118 (2006) 402.
[16] N. Allali, A.M. Marie, M. Danot, C. Geantet, M. Breysse, J. Catal. 156 (1995) 279.
[17] A.S. Rocha, A.C. Faro Jr., L. Oliviero, M.A. Lélias, A. Travert, J. van Gestel, F. Maugé, Catal. Lett. 111 (2006) 27.
[18] L.J. Burcham, J. Datka, E. Wachs, J. Phys. Chem. B 103 (1999) 6015.
[19] J. van Gestel, C. Dujardin, F. Maugé, J.C. Duchet, J. Catal. 202 (2001) 78.
[20] G. Crépeau, V. Montouillout, A. Vimont, L. Mariey, T. Cseri, F. Maugé, J. Phys. Chem. B 110 (2006) 15172.
[21] J.M. Jehng, I.E. Wachs, J. Mol. Catal. 67 (1991) 369.
[22] H. Knozinger, C. Ratnasamy, Catal. Rev. Sci. Eng. 17 (1978) 31.
[23] E.P. Parry, J. Catal. 2 (1963) 371.
[24] S. Khabtou, T. Chevreau, J.C. Lavalley, Micropor. Mater. 3 (1994) 133.
[25] L. Oliviero, A. Vimont, F. Romero, M. Gaillard, F. Maugé, J.C. Lavalley, Phys. Chem. Chem. Phys. 7 (2005) 1861.
[26] P.A. Jacobs, C.F. Heylen, J. Catal. 34 (1974) 267.
[27] C. Morterra, G. Cerrato, G. Meligrana, Langmuir 17 (2001) 7053.
[28] M.I. Zaki, H. Knözinger, Mater. Chem. Phys. 17 (1987) 201.
[29] K. Hadjiivanov, G. Vayssilov, Adv. Catal. 47 (2002) 307.
[30] O. Cairon, T. Chevreau, J.C. Lavalley, J. Chem. Soc. Faraday Trans. 94 (1998) 3039.
[31] J.M. Jehng, I.E. Wachs, Catal. Today 8 (1990) 37.
[32] F. Maugé, A. Vallet, J. Bachelier, J.C. Duchet, J.C. Lavalley, J. Catal. 162 (1996) 88.
[33] M. Angulo, F. Maugé, J.C. Duchet, J.C. Lavalley, Bull. Soc. Chim. Belg. 96 (1987) 925.
[34] A. Travert, C. Dujardin, F. Maugé, E. Veilly, S. Cristol, J.F. Paul, E. Payen, J. Phys. Chem. B 110 (2006) 1261.
[35] J. van Gestel, J. Leglise, J.C. Duchet, Appl. Catal. A 92 (1992) 143.